Science and Technology Indonesia
e-ISSN:2580-4391 *p*-ISSN:2580-4405
Vol. 9, No. 2, April 2024

Research Paper

Synthesis of Zn/SBA-15 from Rice Husk Ash Using Sonochemical Methods as a Quercetin Drug Delivery Matrix

Yulyani Nur Azizah[1]*, Haddiana[1], Tarso Rudiana[1,2]

[1]*Department of Chemistry, Faculty of Science and Technology, Islamic State University Syarif Hidayatullah Jakarta, Tangerang, 15412, Indonesia*
[2]*Department of Chemistry, Faculty of Math and Science, Universitas Mathla'ul Anwar, Padeglang, 42273, Indonesia*
***Corresponding author**: yulyani@uinjkt.ac.id

Abstract
Quercetin is a drug candidate with bioavailability but currently limited, necessitating the use of a delivery matrix, such as Santa Barbara Amorphous-15 (SBA-15). Rice husk ash, containing a significant amount of silica, served as a precursor in the synthesis of SBA-15, which can be functionalized with nanoparticles, including zinc, using sonochemical methods. Therefore, this study aimed to synthesize Zn/SBA-15 using sonochemistry and evaluate the potential as a drug delivery matrix for quercetin. SBA-15 was formed by sonication of a sodium silicate from rice husk and pore director Pluronic P-123, followed by impregnating Zn at 2%, 4%, and 6% w/w. The characterization of X-ray diffraction (XRD) and fluorescence (XRF) showed a broad peak at 2θ 18–30° with Zn levels of 1.89%, 3.69%, and 5.06%. Furthermore, the analysis of transmission electron microscopy (TEM) showed the presence of Zn nanoparticles with a range size of 4-14 nm. *In vitro* drug delivery experiments were carried out using Zn/SBA-15 at concentrations of 1:1 and 1:2 to quercetin. The *in vitro* test results for a drug loading of quercetin with Zn/SBA-15 6% 1:1 was 28.30 mg/g. The encapsulation efficiency was 10.96% and the drug release reached 33.64% after 240 minutes.

Keywords
Drug Delivery, Rice Husk Ash, SBA-15, Quercetin, Zinc

Received: 8 January 2024, Accepted: 23 March 2024
https://doi.org/10.26554/sti.2024.9.2.480-486

1. INTRODUCTION

Quercetin is gaining attention in studies due to the biological properties (Xiao et al., 2018). This flavonoid shows potential benefits for skin health, such as anti-aging and antibacterial properties. However, the decreased bioavailability of quercetin resulted in a challenge for topical administration or application on the skin (Wadhwa et al., 2022). The use of mesoporous materials as drug carriers provides a solution to several challenges related to insufficient solubility and bioavailability (Popova et al., 2016). SBA-15, or Santa Barbara Amorphous-15, is a type of mesoporous material with a hexagonal pore arrangement. The large pores of this material allow for easy access to large drug molecules (Martínez Carmona et al., 2016; Owens et al., 2016). According to a previous study, SBA-15 mesopore carriers contained 35-45 wt% quercetin and released the entire amount of the drug (Popova et al., 2016).

SBA-15 could be easily functionalized on its surface. For instance, mesoporous silica could be modified with zinc to administer topical medication because of its property as a convenient transition metal with antimicrobial characteristics (Rizzotto, 2012; Trendafilova et al., 2017). Zinc ions have a significant tendency to bind and generate chelating donor ligands in organic molecules used as agents for delivering drugs (Mendiguchia et al., 2015). A previous study showed that the loaded amount of quercetin was higher for zinc-containing samples (Popova et al., 2016).

Commercial materials, including Tetraethoxysilane (TEOS), serve as a silica source when synthesizing SBA-15 (Jarmolińska et al., 2020). Exploring substitutes for silica sourced from natural materials, such as rice husk ash provides great potential, as the use of TEOS incurs significant expenses (Rahmat et al., 2016). Agricultural waste, such as rice husks, is abundant in Indonesia and the potential has not been fully maximized. Nzereogu et al. (2023) showed that thermal degradation processes yield rice husk ash with 85% to 95% silica content, providing sample opportunity for exploitation.

SBA-15 was commonly synthesized through hydrothermal methods (Thahir et al., 2019). However, sonochemical methods provide several advantages over hydrothermal, such as cost-effectiveness, energy efficiency, and environmental sustainability. The synthesis of SBA-15 using the sonochemical method occurs rapidly at room temperature, while the hy-

drothermal method requires over 100-120 °C for 24 hours (Bai et al., 2020). Suyanta and Mudasir (2022) reported that the characteristics of the synthesized SBA-15 using the 30-minute sonication method are quite comparable to hydrothermal methods using TEOS. Therefore, this study aimed to synthesize SBA-15 from rice husk ash using sonochemical methods, as well as investigate the effect of varying levels of Zn impregnation on the mesoporous material used as a drug delivery agent for Quercetin. Analysis was carried out on *in vitro* activities, such as scrutinizing drug loading and encapsulation efficacy. Additionally, the release of quercetin was assessed using a UV-Vis spectrophotometer.

2. EXPERIMENTAL SECTION

2.1 Materials

The materials used included rice husk (Tamanku. ID), 33% hydrochloric acid solution, Pluronic P-123 (Merck), sodium hydroxide (Merck), ethanol (Merck), zinc acetate dihydrate (Merck), quercetin (Merck), phosphate buffer pH 5.5 (Merck) and distilled water. The instrumentations used were furnace (Vulcan A-550), oven (Memmert), sonicator (Auguri LW 4000), hot plate stirrer (Thermo Scientific), centrifuge (Hettich EBA 20), X-ray diffraction (XRD) (Shimadzu-7000), fluorescence (PANalytical Type Minipal 4), Fourier Transform Infrared (Shimadzu Type IRPrestige 21), Low-Resolution Transmission Electron Microscope (HT7700), and UV-Vis spectrophotometer (Perkin Elmer lambda 25).

2.2 Methods

2.2.1 Silica Extraction from Rice Husk

Rice husks were washed and oven-dried, then carbonized at 60 °C for three hours in a furnace. Subsequently, 100 grams of rice husk ash were dissolved in 125 mL of 1.6 M hydrochloric acid and stirred at 60 °C for three hours. The mixture was filtered, rinsed with distilled water, and the residue was dried and calcined at 600 °C for another six hours (Suyanta and Mudasir, 2022).

2.2.2 Synthesis and Activation of SBA-15

A mixture of 8 grams of silica extract obtained from rice husk ash and 10 grams of NaOH in a beaker containing 100 milliliters of distilled water was prepared. The solution was stirred for 2 hours at 80 °C, followed by incubation for 12 hours to form a sodium silicate gel. Afterward, pluronic P-123 (3.9 mL) was combined with 100 milliliters of 1.6 M HCl and heated while stirring at 45 °C until dissolved. This was followed by the addition of 100 milliliters of sodium silicate to the Pluronic P-123 solution and sonicated for 30 minutes at room temperature. The solution was heated to 60 °C for one hour before being filtered and then rinsed with both distilled water and ethanol until the pH reached neutrality. The product was then rinsed and filtered with distilled water until a neutral pH water was obtained and then left to dry for 12 hours at 110 °C. The remaining material was desiccated and subsequently annealed at 500 °C for 6 hours (Suyanta and Mudasir, 2022).

After treatment with 150 mL of 18% HCl, the 2 g SBA-15 sample was stirred at 400 rpm for 24 hours. Subsequently, the sample was rinsed and filtered using distilled water to achieve a neutral pH. The remaining residue was dried for 12 hours at 110 °C.

2.2.3 Functionalization of SBA-15

SBA-15 was functionalized using Zinc acetate dihydrate in 2%, 4%, and 6% (w/w) masses mixed into 1 mL of ethanol. This procedure was followed by incorporating 300 mg of mesoporous SBA-15, and the resultant mixture was sonicated at room temperature. Samples were calcined at 500 °C for 3 hours and the final product was characterized by XRD, XRF, and LRTEM (Trendafilova et al., 2017).

2.2.4 Functional Group Analysis Using FTIR

The Zn-Qu/SBA15 sample was crushed with KBr in a 1:10 ratio. Afterward, the sample was measured at a wave number range of 4000-500 cm^{-1}.

2.2.5 Loading Test and Drug Encapsulation Efficiency

Quercetin at 2 mg and 4 mg were dissolved in 100 mL of ethanol. The solution was then subjected to centrifugation at 2500 rpm for 45 minutes and allowed to rest for 1.5 hours. The supernatant obtained was drawn off using a pipette (1 mL), and subsequently diluted with 100 mL of ethanol. Initial concentration (C_0) was measured using a UV-Vis spectrophotometer at a predetermined wavelength.

Zn/SBA-15 and quercetin at mass ratios of 1:1 and 1:2 were dissolved in 100 mL of ethanol and treated according to the C_1 procedure. The concentration of quercetin was determined using the standard calibration curve equation in ethanol, enabling the calculation of drug loading and encapsulation efficiency (Zaharudin et al., 2020).

$$\text{Encapsulation Efficiency}\,(\%) = \frac{(C_0 - C_1)}{C_0} \times 100\% \quad (1)$$

$$\text{Drug Loading}\,(\frac{mg}{g}) = \frac{(C0 - (C_1 \times V_1))V_0}{w} \quad (2)$$

Notes:
C_1: Drug levels after dissolving in solvent and Zn/SBA-15 (mg/L)
C_0: Drug concentration after dissolving the solvent (mg/L)
V_1: Final volume of supernatant (L)
V_0: Volume of solvent (L)
W: Mass of Zn/SBA-15 (g)

The solution C_1 was tested for drug loading and encapsulation efficiency using a UV-Vis spectrophotometer. The measurements between 200 and 600 nm were taken and the maximum wavelength shift was used for analysis

Table 1. Element Composition of Zn/SBA-15

Sample	% Mass of the Element						
	Si	Zn	Al	S	Ca	Fe	Cl
SBA-15/Zn 2%	61,4	1,89	0,168	0,056	0,066	0,029	0,015
SBA-15/Zn 4%	61,3	3,69	0,174	0,014	0,061	0,030	0,058
SBA-15/Zn 6%	56,8	5,06	0,171	0,019	0,049	0,027	0,069

Table 2. FTIR Results of Qu-Zn/SBA-15 6% 1:1 Compared with the Results of Other Studies

Functional Groups	Wavenumbers (cm^{-1})		
	Quercetin (Kalinowska et al., 2016)	Qu-Zn/SBA-15 (Trendafilova et al., 2017)	Qu-Zn/SBA-15 (this research)
v C=O	1672	1655	1661
v C−OH	1362	1380	1321

2.2.6 *In-vitro* Drug Release Test

The sample with the greatest percentage loading and encapsulation was mixed in 1 mL of ethanol and heated until the solvent evaporated, then dried at 40 °C overnight. The sample incubated with 100 mL of pH 5.5 phosphate buffer while being stirred at 300 rpm, at a temperature of 37 °C. At 30, 60, 120, 180, and 240-minute intervals, 1 mL was extracted from the release medium and subsequently diluted to 50 mL. UV-Vis spectroscopy analysis was carried out at 367 nm to calculate the concentration of released quercetin using the standard calibration curve equation at pH 5.5 (Trendafilova et al., 2017). The percentage of quercetin release was determined using Equations (3) and (4).

$$\text{Drug Release} = \frac{C_{quer}\left(\frac{mg}{L}\right) \times FP \times \text{Volume Media}\,(L)}{1000} \quad (3)$$

$$\%\text{Drug Release} = \frac{\text{Drug Release}\,(g)}{\text{Total Quercetin Added}\,(g)} \times 100\% \quad (4)$$

Notes:
FP: Dilution factor
C: Concentration

3. RESULTS AND DISCUSSION

3.1 Characteristics of Synthesized SBA-15

The process of calcination and leaching of rice husk ash was aimed at eliminating impurities, including metal oxides or organic materials, to improve the quality of silica (SiO_2) (Nzereogu et al., 2023). Consistent with a previous study by Morales Paredes et al. (2023), the rice husk ash obtained was white due to the decrease in impurity concentration. According to Kikuchi et al. (2016), the sodium hydroxide dissolved the silica extract from rice husk ash to produce sodium silicate, as shown in Equation (5).

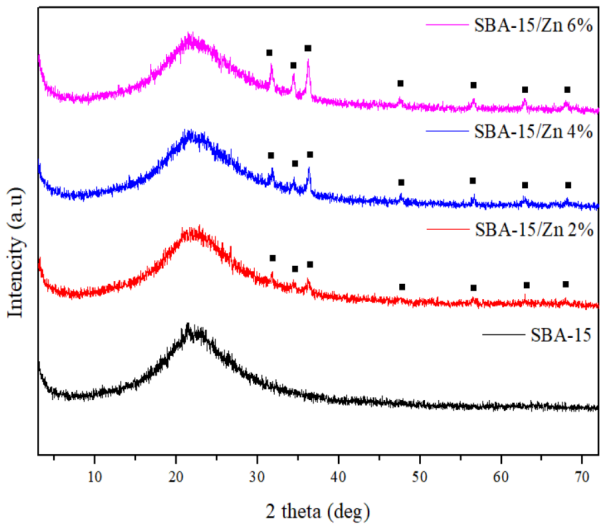

Figure 1. Diffractogram Pattern of Zn Impregnated SBA-15

$$SiO_2 + 2NaOH \rightarrow Na_2SiO_3 + H_2O\ (\Delta H = -85\ \text{kJ mol}^{-1}) \quad (5)$$

The sodium silicate was used to synthesize SBA-15, using pluronic P123 as the template. The synthesized SBA-15 was activated using HCl since it created an acidic environment, resulting in an abundance of H^+ ions and formation of silanol groups. These silanol groups act as Bronsted acids and interact with metal ions (Tsyganenko et al., 2000). Figure 1 shows the diffractogram pattern of SBA-15, with broad and no sharp peaks within the 2θ range of 18-30°. A similar pattern was found in previous studies where the synthesis of SBA-15 included TEOS precursors through hydrothermal or sonication methods. This resulted in a broad peak at 2θ of 18-35°, reflecting an amorphous silica structure (Filiz and Balci, 2019).

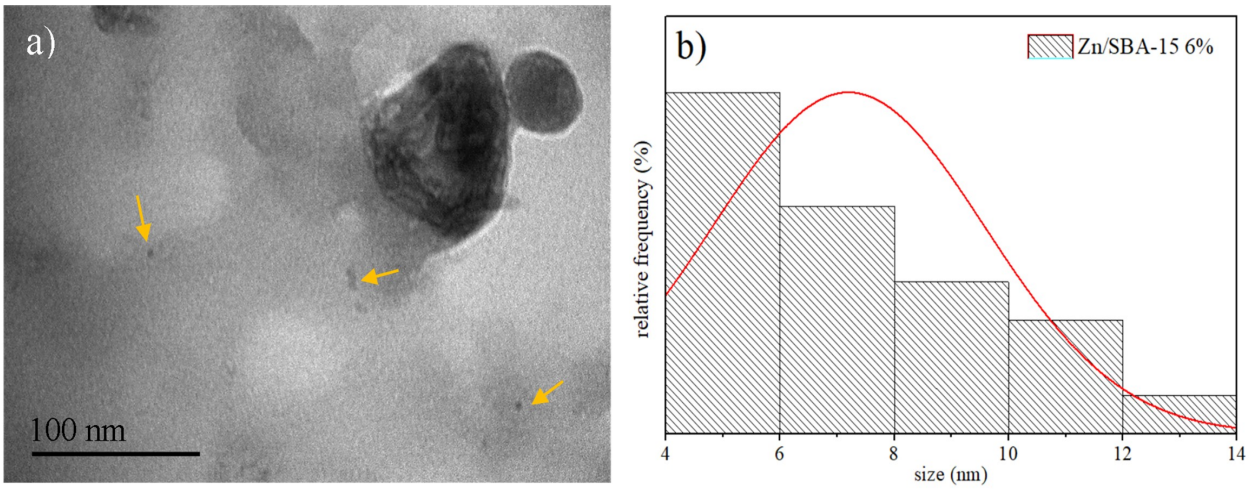

Figure 2. a) Nanoparticles Zn in SBA-15 Under 100 nm Scale, b) Nanoparticles Distribution Size

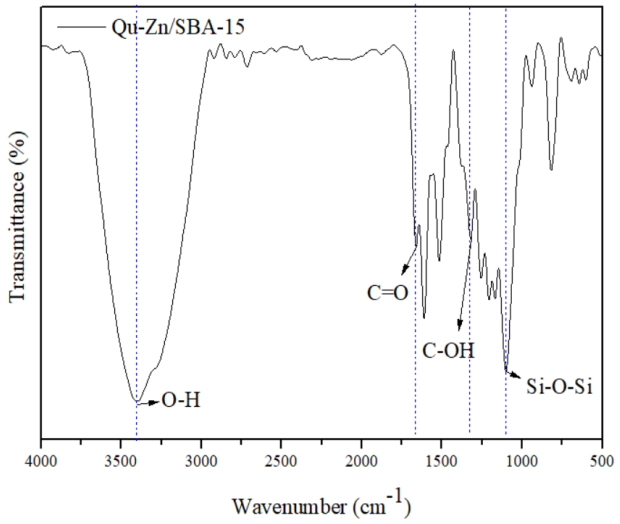

Figure 3. FTIR Spectrum of Quercetin Chelation with Zn/SBA-15

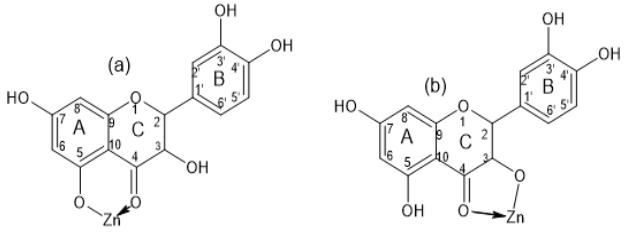

Figure 4. Chelation of Zn with Quercetin: a) Through A and C Ring, b) Involved Only C Ring

The new peaks at 2θ, namely 31°, 34°, 36°, 47°, 56°, 62°, and 68° confirmed effective Zn impregnation in SBA-15, consistent with a previous study (Zhixiong et al., 2014). The signal intensity at the metal's characteristic peak grows with increasing zinc content in SBA-15. The Zn/SBA-15 2% and 6% samples exhibited the highest and lowest amount of silicon (Si) in comparison to others with a percentage of 61.4% and 56.8%, respectively (Table 1). The concentration of zinc introduced to SBA-15 was found to be positively correlated with the quantity impregnated.

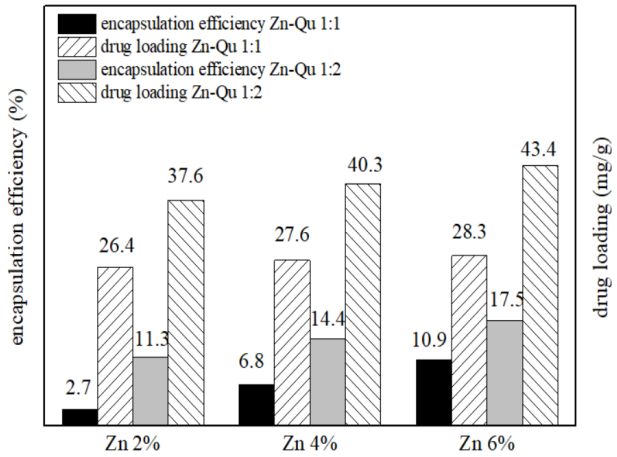

Figure 5. Drug Loading and Encapsulation Efficiency of Zn-Qu/SBA-15 1:1 and 1:2

The XRF result in Table 1 shows that SBA-15 material contains rice husk ash impurities, such as Al, S, Ca, Fe, and Cl (Nasir et al., 2021). The concentration of HCl has a significant impact on the presence of impurities. According to a previous study, a 2 M concentration of HCl can remove up to 95% of impurities (Pote et al., 2022).

The presence of nanoparticles was observed below the 100 nm scale as previously reported (Bhuyan et al., 2015). Figure 2 shows that the Zn nanoparticles remain on the surface of the mesoporous channel. After processing with the ImageJ application, the zinc nanoparticles, ranging in size from 4-

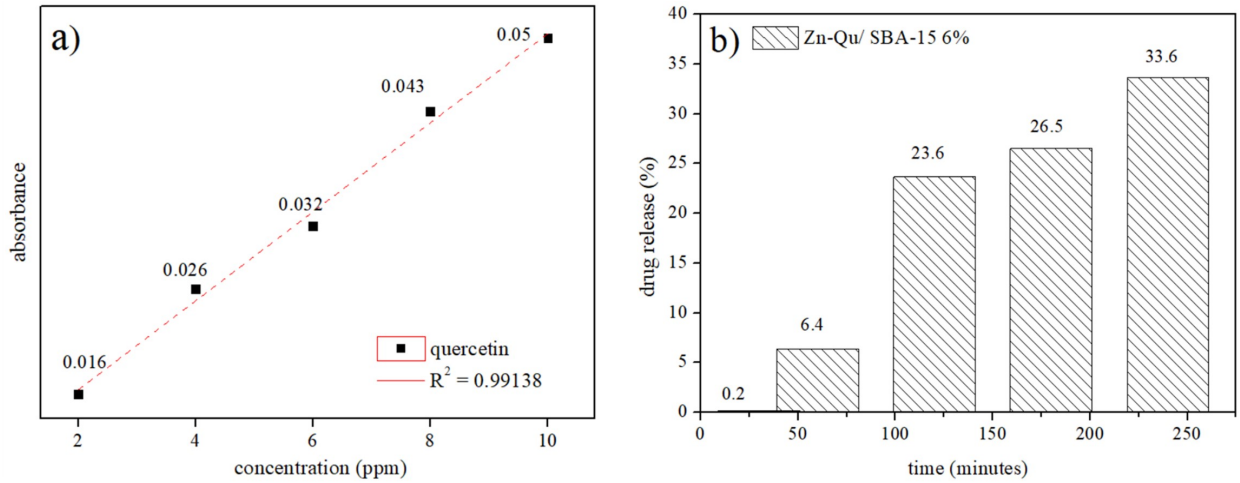

Figure 6. (a) Calibration Curve of a Standard Solution of Quercetin in Phosphate Buffer pH 5.5; and (b) Drug Release of Quercetin in Zn/SBA-15 6% 1:1

14 nm, were distributed onto SBA-15 (Refat et al., 2021). However, the particles have agglomerated on the surface of SBA-15 areas. The hexagonal pore pattern of SBA-15 was only observed in high-resolution TEM measurements, which was not showed in this result.

Figure 3 shows the FTIR results of the Zn/SBA-15 with quercetin ratio of 1:1. The IR spectra show the stretching vibration presence of Si−O−Si and Si−OH from SBA-15 at 1100 cm^{-1} and ~900 cm^{-1}, respectively, as well as O−H derived from water molecules at 3400 cm^{-1} (Khanh Nguyen et al., 2020).

A comparison was made between the functional groups and the parent quercetin to clarify the interaction between quercetin and Zn/SBA-15. The FTIR and previous study results for Qu-Zn/SBA-15 are shown in Table 2. The wave numbers from quercetin were shifted lower at the C=O and C−OH groups, suggesting an interaction between zinc and quercetin (Kalinowska et al., 2016). The result of Kalinowska et al. (2016) showed that the C=O functional group was observed to shift from 1672 cm^{-1} to 1661 cm^{-1}, while the C−OH shifted from 1362 cm^{-1} to 1321 cm^{-1}. This decrease in wave number was attributed to the preference for chelating metal bonds over hydrogen bonds (Azizah et al., 2020).

Based on the FTIR assay results, quercetin showed a tendency to chelate zinc metal at the C=O and C(5)−OH in ring C and A, respectively, as illustriated in Figure 4a, or C(3)–OH in ring C (Figure 4b). According to Refat et al. (2021), C(4)=O carbonyl oxygen atom on the C ring, and the C(3)–OH or C(5)–OH group can coordinate Zn(II) metal ions.

3.2 Drug Loading and Encapsulation Efficiency

The drug-chelating ability of Zn/SBA-15 was measured at band I with a wavelength of 370 nm, which showed the absorption of the cinnamoyl B ring (Elvira et al., 2018). Based on absorbance measurement, the amount of drug loading increased in direct proportion to the concentration (%) of zinc in Zn/SBA-15, as shown in Figure 5. The highest loading values were observed in 6% Zn/SBA-15 with quercetin at ratios of 1:1 and 1:2, at 28.3 mg/g and 43.41 mg/g respectively. According to Trendafilova et al. (2017), increasing the zinc concentration to 6% resulted in an increase in drug loading. This increase was also observed in the study conducted by Popova et al. (2016).

The encapsulation efficiency was found to increase with increasing zinc concentration in SBA-15. Furthermore, the maximum encapsulation efficiency of 17.5% was observed in Zn/SBA-15 6% with a 1:2 quercetin ratio, as shown in Figure 5. The minimum encapsulation efficiency of 2.7% was recorded in Zn/SBA-15 2%. According to Patel et al. (2014), particle size was considered an important parameter as the size of the particle affects its physical stability in colloidal suspension. Adrover et al. (2020) also showed that a decrease in the particle size of the drug carrier matrix results in a decrease in efficiency.

3.3 Drug Release Result

A study conducted by Trendafilova et al. (2017) showed that the release of quercetin takes place in a phosphate buffer solution with a pH of 5.5, corresponding to the physiological pH of the skin. Quercetin exhibited a higher release rate under acidic pH conditions (Alkahtani et al., 2022). The concentration of the release quercetin was calculated based on the standard curves prepared in pH 5.5 solution as shown in Figure 6a. Higher levels of zinc result in a slower release of quercetin, possibly due to the complexation of quercetin. In comparison with previous studies (Trendafilova et al., 2017), 4% of zinc needed less than an hour to release the drug. In this study, 6% of zinc required more than 240 minutes to release 30% of quercetin. However, the content of quercetin increases due to the solubility of the Zn-quercetin complex in water (Uskoković Marković et al., 2020).

The drug release was 0.2% after the first 30 minutes, as

shown in Figure 6b, and later increased to 33.6% at the 240th minute. Previous studies have shown that SBA-16/Zn 4% can release up to 70% of quercetin (Popova et al., 2016). The size of pores in carriers was commonly acknowledged to have a significant impact on drug release. This is exemplified by the smaller mesopore size of SBA-15 when compared to SBA-16 (Adrover et al., 2020). In several studies, the percentage of drug release from functionalized SBA-15 was lower due to increased inhibition of drug exit. Furthermore, the slower release of quercetin in samples containing Zn may be attributed to complexation in the cavity, formation of zinc oxide, and narrower pores entrance (Popova et al., 2016). The slow-release formulations can be applied topically to the skin. Consistent with the study conducted by Kajbafvala et al. (2018), the slow release of quercetin shows significant usefulness in controlled-release applications, such as topical sunscreen formulations, as it provides long-term UV protection.

4. CONCLUSIONS

The sonochemical method was applied to synthesize SBA-15 using a silica precursor obtained from rice husk ash. Analysis from XRD showed a formation of amorphous SBA-15 with wide peaks within the 2θ 18-30° range. The impregnation of zinc within SBA-15 had a significant effect on the composite elements, showing zinc quantities of 1.89%, 3.69%, and 5.06% in Zn/SBA-15 2%, 4%, and 6% (w/w), respectively. Zinc particles were successfully impregnated on the SBA-15 pore and surface in a range size of 4-14 nm. The FTIR analysis showed that quercetin interacted through chelation with Zn/SBA-15 at 1661 and 1321 cm^{-1}. The result of *in vitro* testing showed that the highest quercetin drug loading reached 43.4 mg/g with an encapsulation efficiency of 17.5% in 6% Zn/SBA-15 with a ratio of 1:2 to quercetin.

5. ACKNOWLEDGMENT

The authors are grateful to the Rector of State Islamic University Syarif Hidayatullah Jakarta for funding this study through LPPM 2024.

REFERENCES

Adrover, M. E., M. Pedernera, M. Bonne, B. Lebeau, V. Bucalá, and L. Gallo (2020). Synthesis and Characterization of Mesoporous SBA-15 and SBA-16 As Carriers to Improve Albendazole Dissolution Rate. *Saudi Pharmaceutical Journal*, **28**(1); 15–24

Alkahtani, S., S. Alarifi, N. H. Aljarba, H. A. Alghamdi, and A. A. Alkahtane (2022). Mesoporous SBA-15 Silica–Loaded Nano-Formulation of Quercetin: A Probable Radio-Sensitizer for Lung Carcinoma. *Dose-Response*, **20**(1); 1–10

Azizah, Y. N., I. Mulyani, D. Wahyuningrum, and D. N. Bima (2020). Synthesis, Characterization and Antioxidant Activity of Kobalt (II)-Hydrazone Complex. *Educhemia (Jurnal Kimia dan Pendidikan)*, **5**(2); 119–133

Bai, K., J. Hao, Y. Yang, and A. Qian (2020). The Effect of Hydrothermal Temperature on the Properties of Sba-15 Materials. *Heliyon*, **6**(8); 04436

Bhuyan, D., A. Gogoi, M. Saikia, R. Saikia, and L. Saikia (2015). Facile Synthesis of Gold Nanoparticles on Propylamine Functionalized SBA-15 and Effect of Surface Functionality of Its Enhanced Bactericidal Activity against Gram Positive Bacteria. *Materials Research Express*, **2**(7); 075402

Elvira, K., E. Fachriyah, and D. Kusrini (2018). Isolation of Flavonoid Compounds from Eceng Gondok (*Eichhornia crassipes*) and Antioxidant Tests with Dpph (1, 1-Diphenyl-2-Picrylhydrazyl) Method. *Jurnal Kimia Sains dan Aplikasi*, **21**(4); 187–192

Filiz, A. and S. Balci (2019). Structural Variations in SBA-15 by Copper Incorporation and a Test in Catalytic Wet Peroxide Oxidation of Phenol. *Gazi University Journal of Science*, **32**(1); 91–102

Jarmolińska, S., A. Feliczak Guzik, and I. Nowak (2020). Synthesis, Characterization and Use of Mesoporous Silicas of the Following Types SBA-1, SBA-2, HMM-1 and HMM-2. *Materials*, **13**(19); 4385

Kajbafvala, A., A. Salabat, and A. Salimi (2018). Formulation, Characterization, and *In vitro/Ex vivo* Evaluation of Quercetin-Loaded Microemulsion for Topical Application. *Pharmaceutical Development and Technology*, **23**(8); 741–750

Kalinowska, M., G. Świderski, M. Matejczyk, and W. Lewandowski (2016). Spectroscopic, Thermogravimetric and Biological Studies of Na (I), Ni (II) and Zn (II) Complexes of Quercetin. *Journal of Thermal Analysis and Calorimetry*, **126**(1); 141–148

Khanh Nguyen, Q. N., N. T. Yen, N. D. Hau, and H. L. Tran (2020). Synthesis and Characterization of Mesoporous Silica SBA-15 and ZnO/SBA-15 Photocatalytic Materials from the Ash of Brickyards. *Journal of Chemistry*, **2020**; 1–8

Kikuchi, S., N. Koga, H. Seino, and S. Ohno (2016). Experimental Study and Kinetic Analysis on Sodium Oxide–Silica Reaction. *Journal of Nuclear Science and Technology*, **53**(5); 682–691

Martínez Carmona, M., M. Colilla, M. L. Ruiz González, J. M. González Calbet, and M. Vallet Regí (2016). High Resolution Transmission Electron Microscopy: A Key Tool to Understand Drug Release from Mesoporous Matrices. *Microporous and Mesoporous Materials*, **225**; 399–410

Mendiguchia, B. S., I. Aiello, and A. Crispini (2015). Zn (II) and Cu (II) Complexes Containing Bioactive O, O-Chelated Ligands: Homoleptic and Heteroleptic Metal-Based Biomolecules. *Dalton Transactions*, **44**(20); 9321–9334

Morales Paredes, C. A., I. Rodríguez Linzán, M. D. Saquete, R. Luque, S. M. Osman, N. Boluda Botella, and R.-D. J. Manuel (2023). Silica-Derived Materials from Agro-Industrial Waste Biomass: Characterization and Comparative Studies. *Environmental Research*, **231**(1); 116002

Nasir, I., N. Ameram, A. Arlina, S. R. Hassan, N. A. C. Zaudin, and J. M. Sapari (2021). A Review of Rice Husk Silica As a

Heterogeneous Catalyst Support. *Journal of Metals, Materials and Minerals*, **31**(4); 1–12

Nzereogu, P., A. Omah, F. Ezema, E. Iwuoha, and A. Nwanya (2023). Silica Extraction from Rice Husk: Comprehensive Review and Applications. *Hybrid Advances*, **4**; 100111

Owens, G. J., R. K. Singh, F. Foroutan, M. Alqaysi, C. M. Han, C. Mahapatra, H. W. Kim, and J. C. Knowles (2016). Sol–Gel Based Materials for Biomedical Applications. *Progress in Materials Science*, **77**; 1–79

Patel, P. J., M. C. Gohel, and S. R. Acharya (2014). Exploration of Statistical Experimental Design to Improve Entrapment Efficiency of Acyclovir in Poly (d, l) Lactide Nanoparticles. *Pharmaceutical Development and Technology*, **19**(2); 200–212

Popova, M., I. Trendafilova, Á. Szegedi, J. Mihály, P. Németh, S. G. Marinova, H. A. Aleksandrov, and G. N. Vayssilov (2016). Experimental and Theoretical Study of Quercetin Complexes Formed on Pure Silica and Zn-Modified Mesoporous MCM-41 and SBA-16 Materials. *Microporous and Mesoporous Materials*, **228**; 256–265

Pote, L. L., P. R. R. Sanam, and G. Latumakulita (2022). Synthesis and Characterization of Silica Gel of Waste Agate From The Nian Village of Timor Tengah Utara Regency Using Sol Gel Method. *Indonesian Journal of Chemical Research*, **7**(2); 9–17

Rahmat, N., F. Hamzah, N. Sahiron, M. Mazlan, and M. M. Zahari (2016). Sodium Silicate As Source of Silica for Synthesis of Mesoporous SBA-15. In *IOP Conference Series: Materials Science and Engineering*, volume 133. IOP Publishing, page 012011

Refat, M. S., R. Z. Hamza, A. M. A. Adam, H. A. Saad, A. A. Gobouri, F. S. Al Harbi, F. A. Al Salmi, T. Altalhi, and S. M. El Megharbel (2021). Quercetin/Zinc Complex and Stem Cells: A New Drug Therapy to Ameliorate Glycometabolic Control and Pulmonary Dysfunction in Diabetes Mellitus: Structural Characterization and Genetic Studies. *PLoS One*, **16**(3); e0246265

Rizzotto, M. (2012). *A Search for Antibacterial Agents*, volume 10, chapter Metal Complexes As Antimicrobial Agents. InTech: Rijeka, Croatia, page 45651

Suyanta, S. and M. Mudasir (2022). Optimizing Rice Husk Silica Mass and Sonication Time for a More Efficient and Environmentally Friendly Synthesis of SBA-15. *Indonesian Journal of Chemistry*, **22**(4); 1090–1106

Thahir, R., A. W. Wahab, N. L. Nafie, and I. Raya (2019). Synthesis of High Surface Area Mesoporous Silica SBA-15 by Adjusting Hydrothermal Treatment Time and the Amount of Polyvinyl Alcohol. *Open Chemistry*, **17**(1); 963–971

Trendafilova, I., A. Szegedi, J. Mihály, G. Momekov, N. Lihareva, and M. Popova (2017). Preparation of Efficient Quercetin Delivery System on Zn-Modified Mesoporous SBA-15 Silica Carrier. *Materials Science and Engineering*, **73**; 285–292

Tsyganenko, A., E. Storozheva, O. Manoilova, T. Lesage, M. Daturi, and J. Lavalley (2000). Brønsted Acidity of Silica Silanol Groups Induced by Adsorption of Acids. *Catalysis Letters*, **70**; 159–163

Uskoković Marković, S., M. Milenković, and L. Pavun (2020). Zinc-Quercetin Complex: From Determination to Bioactivity. *Acta Agriculturae Serbica*, **25**(50); 113–120

Wadhwa, K., V. Kadian, V. Puri, B. Y. Bhardwaj, A. Sharma, R. Pahwa, R. Rao, M. Gupta, and I. Singh (2022). New Insights into Quercetin Nanoformulations for Topical Delivery. *Phytomedicine Plus*, **2**(2); 100257

Xiao, L., G. Luo, Y. Tang, and P. Yao (2018). Quercetin and Iron Metabolism: What We Know and What We Need to Know. *Food and chemical toxicology*, **114**; 190–203

Zaharudin, N. S., E. D. M. Isa, H. Ahmad, M. B. A. Rahman, and K. Jumbri (2020). Functionalized Mesoporous Silica Nanoparticles Templated by Pyridinium Ionic Liquid for Hydrophilic and Hydrophobic Drug Release Application. *Journal of Saudi Chemical Society*, **24**(3); 289–302

Zhixiong, L., N. Wei, W. Hua, and G. Wengui (2014). Direct Syntheses of Cu-Zn-Zr/SBA-15 Mesoporous Catalysts for CO_2 Hydrogenation to Methanol. *Chemical Journal of Chinese Universities-Chinese*, **35**(12); 2616–2623

